

A New Approach to Analyzing Airborne Delay

Tim Myers^{*}, Michael Brennan[†], and Mark Klopfenstein[‡]

Metron Aviation, Inc., Herndon, VA, 20170

Numerous techniques exist for measuring airborne delay. These techniques vary in the ways in which airborne delay is modeled and quantified, and in how delay is measured. We define a new approach for measuring airborne delay which expands our ability to analyze problems in airspace congestion and the different types of Air Traffic Control action used to manage airborne traffic. We develop mathematical models to detect and record where and when airborne delays occur in the form of vectoring, directs, airspeed controls, and amendments. Airborne delays are computed between consecutive position updates using historical Enhanced Traffic Management System flight data and Rapid Update Cycle winds aloft data. We present initial results of applying these airborne delay estimation techniques. Finally, we introduce the application of these techniques to analyzing airborne delay propagation and the dependence of airborne delay on weather using various visualization techniques.

Nomenclature

\mathbf{a}	= displacement vector between previous and current waypoint crossing points
a_a	= rate of acceleration for estimated groundspeed profile
a_d	= rate of deceleration for estimated groundspeed profile
D	= distance flown based on estimated groundspeed profile
d	= net impact of airborne delay from vectoring, directs, airspeed controls, and route amendments
d_{amd}	= airborne delay due to route amendments
d_{asp}	= airborne delay due to airspeed controls
d_{dir}	= airborne delay due to directs
d_{vect}	= airborne delay due to vectoring
L	= length of filed flight plan
\mathbf{p}	= displacement vector between previous and current flight positions
S	= equivalent length of the current route between consecutive waypoint bisector crossings
\mathbf{s}	= displacement vector between previous and next waypoints in the current route
v_a	= inferred actual airspeed
v_i	= intended airspeed from filed flight plan
v_r	= runway groundspeed for estimated groundspeed profile
v_c	= cruise groundspeed for estimated groundspeed profile
t_a	= duration of acceleration phase for estimated groundspeed profile
t_c	= duration of cruise phase for estimated groundspeed profile
t_d	= duration of deceleration phase for estimated groundspeed profile
t_{ete}	= estimated duration of flight from filed flight plan
Δt	= change in time between previous and current flight positions
α	= distance between current position and previous waypoint, $ \mathbf{a} $
β	= distance between current position and current route segment
δ	= $\alpha - S$
ϵ	= distance reduction threshold

^{*} Senior Analyst, Research and Analysis Department, 131 Elden Street, Suite 200, AIAA Member.

[†] Chief Scientist, Business Development, 131 Elden Street, Suite 200, AIAA Member.

[‡] Program Manager, Research and Analysis Department, 131 Elden Street, Suite 200, AIAA Member.

I. Introduction

A long-standing impediment to understanding traffic flow, problems in airspace congestion, and the effectiveness and results of traffic management initiatives has been a lack of knowledge about where and when flights are delayed while airborne. The objective of our research is to design and implement a methodology for computing and recording when and where flights take airborne delay by comparing the intended flight progress as expressed in the currently-active flight plan against the actual progress as measured by the positions, altitudes, and speeds reported in the Enhanced Traffic Management System (ETMS) position report (TZ) messages.

Airborne delays are a necessary element of Traffic Flow Management (TFM). To maintain safe separation, merge traffic, and avoid conflicts requires Air Traffic Control (ATC) actions that may result in airborne delay. ATC uses a number of tools to manage airborne demand including vectoring, airspeed controls, and route amendments. These and other ATC control actions can result in airborne delays. Understanding how these delays occur will provide valuable information regarding system performance that among other benefits will enable us to:

- Identify consistent patterns of delay for specific areas at specific times to aid in improved routing decisions and to illuminate TFM and ATC problems
- Investigate methods for improving flight time predictability by estimating anticipated airborne delays
- Examine the role of airborne delays in Ground Delay Program (GDP) and Airspace Flow Program (AFP) delivery problems by determining when delivery was reduced due to airborne delays
- Evaluate the feasibility of estimating airborne delays in real time, to provide updated delay information for all flights and geographically identify areas where delays are being incurred

Previous work has established the difficulty in identifying where and when en route delays occur [2]. Delay estimates have been made using expected flight time (ETE) data in an attempt to identify flights that were airborne longer than expected [3]. These attempts are limited in that they do not provide insight into where or when delays occur during flight. Approaches have also included the evaluation of excess distance flown within particular regions of airspace [4][5], including Air Route Traffic Control Centers (ARTCC or Center) and sectors. Another method of en route delay estimation explores the use of trajectory prediction (TP) model data as a basis for identifying where and when airborne delays occur [6]. In this TP-based approach, a baseline estimated time of arrival (ETA) is computed when a flight first becomes airborne. The ETA is then updated based on the actual flight progress.

Deviations in the updated ETA from the baseline ETA are regarded as en route delay. Finally, other approaches have examined specific airborne delay events such as flights being placed in circular holding patterns [7].

This paper describes an alternative technique for measuring airborne delay, which overcomes many of the limitations found in previous work. Our approach decomposes airborne delay into that due to vectoring, directs, airspeed controls, and airborne amendments. These four components correspond to the primary methods that ATC employs in managing airborne traffic, which gives us insight into their actions.

In the remainder of this paper we describe our methodology for measuring these delay components and the results of our current work to examine patterns in airborne delay and delay propagation.

II. Measuring Airborne Delays

We have developed promising techniques for measuring airborne delays from vectoring, airspeed controls, directs (also known as “direct to” routes), and amendments. The advantage of this approach is that it enables the distinction between various types of ATC intervention as well as the identification of where and when airborne delays occurred. This section discusses the four forms of airborne delay and the mathematics used to detect and measure each quantity.

Vectoring Delays

Vectoring delays occur when flights deviate away from their active route. ETMS track (TZ) data were used to define the actual flight path and the filed and amended routes defined the intended flight path. Vectoring can take on the form of path-stretching, S-turns or circular holding as shown in **Figure 1**.

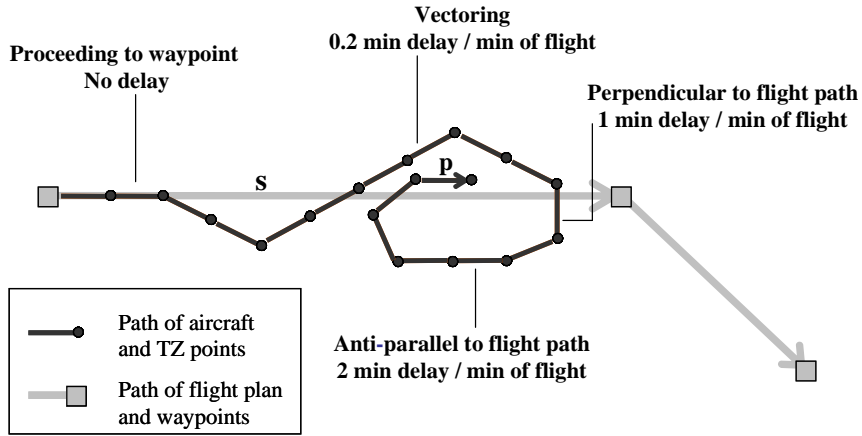


Figure 1. Vectoring delays are measured by comparing the actual flight progress to the progress made along the active route.

Starting from the left in Figure 1, the path runs parallel the flight plan, so no delay is measured. Then the flight is vectored to slow its advance, and only 80% of its actual progress is projected along its intended path, so this would be recorded as taking 0.2 minutes of delay for each one-minute position report. After a few additional heading changes, the flight enters a circular holding pattern at which point the actual path is perpendicular to the flight plan. No progress is made towards the next waypoint when flying perpendicular to the flight plan resulting in one minute of delay per minute of flight. Eventually the flight is back-tracking on its intended course in such a way that each minute of flight is not merely counter-productive but adds another minute to the required time to recover. This produces the maximum vectoring delay of two minutes delay per minute of flight.

In short, vectoring delays are measured by evaluating the portion of the actual flight progress that is directed along the active route towards the next waypoint, which can be determined simply by calculating the angle $\theta(t)$ between the actual and intended flight paths at time t where Δt is inter-TZ time, usually one minute.

$$d_{\text{vect}}(t) = \Delta t(1 - \cos \theta(t)) \quad (1)$$

This method of measuring vectoring delays can also be written in vector form where \mathbf{p} is the displacement vector between the previous and current TZs at time t and \mathbf{s} is the displacement vector along the current waypoint segment of the active route.

$$d_{\text{vect}}(t) = \Delta t(1 - \text{proj}_{\mathbf{s}} \mathbf{p} / |\mathbf{p}|) \quad (2)$$

Identifying the Current Waypoint Segment

Flight plans typically consists of multiple waypoints. We refer to the gap between consecutive waypoints as a waypoint segment. Each waypoint segment may have a different heading. To measure vectoring delays, as well as directs and route amendments described in the following sections, we must first identify the waypoint segment along which the flight is currently traveling. The current waypoint segment defines the intended heading during each portion of flight. **Figure 2** illustrates the bisector method used to identify the current waypoint segment.

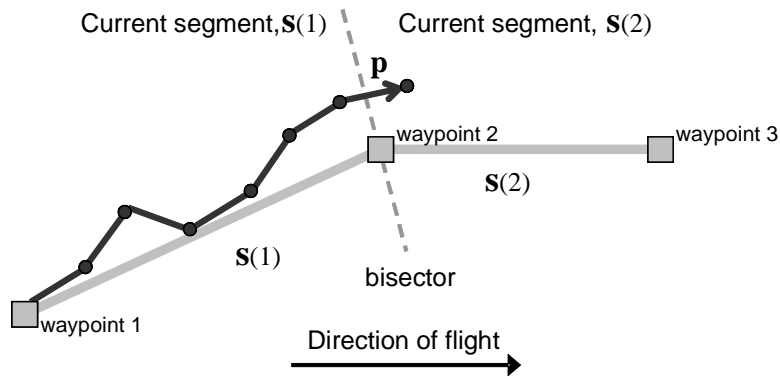


Figure 2. A waypoint is considered passed once the flight is beyond the line that bisects consecutive waypoint segments.

The bisector method simply evaluates whether a flight has passed the bisector between consecutive waypoint segments. The flight in the figure has just passed the bisector at waypoint 2, making $s(2)$ the current waypoint segment. In this example, vectoring delay will now be measured relative to $s(2)$ using Eq. (2). Additional logic was incorporated to augment the bisector method. In **Figure 3** for example, a flight has passed waypoint W2 and is now heading towards W3. The bisector method alone, however, would also indicate that the flight is passed the bisector at W5. As an added constraint in determining whether a new waypoint has been passed, we compute the distance, α , from the previous waypoint as well as the lateral displacement, β , from the current and candidate waypoint segments as depicted in the figure. In particular, a candidate waypoint is deemed passed if and only if

$$\alpha' \beta' < \alpha \beta \quad (3)$$

where α' and β' are the distance and lateral displacement parameters for the candidate waypoint (W5 in this example). Based on this additional level of logic, the flight in the figure would be mapped to the waypoint segment connecting W2 and W3.

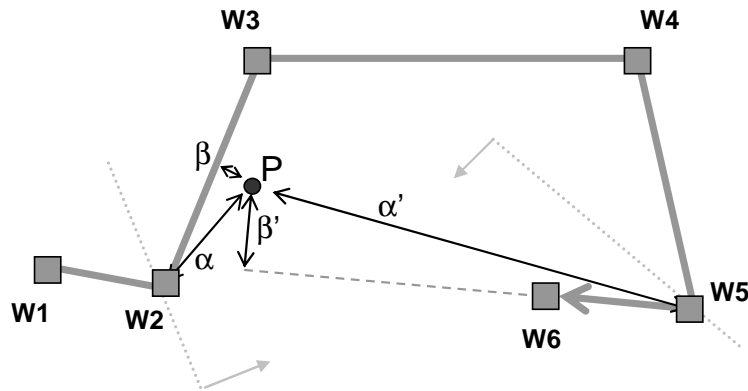


Figure 3. Additional logic is applied for determining whether a new waypoint has been passed

Directs

ATC actions can result in reduced airborne delay. One such action is the issuing of a direct, which allows a flight to short-circuit part of its route. Directs are a special form of vectoring, which are dealt with separately. The approach to measuring vectoring delays described in the previous section is applicable only for evaluating the impact of vectoring intended to slow a flight's advance along its route. In particular, vectoring delays measured from Eq. (2) will always be between 0 and $2\Delta t$. A different approach was developed for evaluating the special case of vectoring intended to reduce airborne delay.

The occurrence of a direct is checked for each time a waypoint is passed by comparing the planned and actual flown distance between consecutive waypoint bisector crossings. **Figure 4** shows a flight on a direct to waypoint $n+2$ with the locations of consecutive waypoint bisector crossing denoted with an "X". A direct has been detected given that the actual distance flown between consecutive waypoint crossings, depicted as the length $|a|$, is less than the equivalent planned distance along that portion of the route represented by the length S . Directs can also be detected between nonconsecutive waypoints. For example, if the flight in the figure were to cross the bisector at waypoint $n+2$ prior to waypoint $n+1$ then S would include the lengths of multiple waypoint segments.

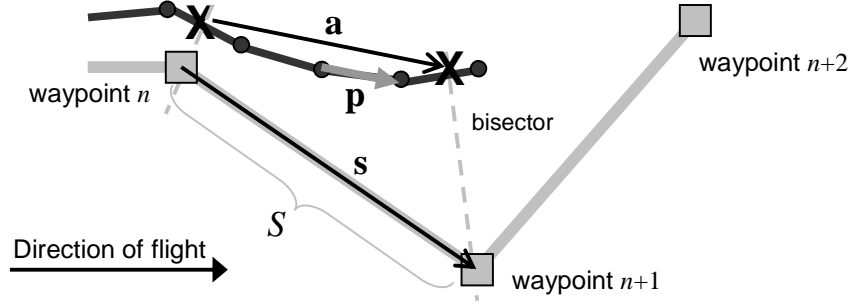


Figure 4. Directs are detected by comparing the actual and planned distances flown between consecutive waypoints.

The delay reduction associated with a direct is measured using the following steps.

Step 1: Upon crossing each new waypoint bisector, evaluate the difference between the planned and actual distances flown:

$$\delta = |\mathbf{a}| - S. \quad (4)$$

Step 2: If $\delta < -\epsilon$, where ϵ is a threshold amount, then a direct has occurred. A value of $\epsilon = 1$ nmi was found to be acceptable.

Step 3: For all TZs between the waypoint crossing points, the benefit of the direct is computed to be:

$$d_{dir}(t) = \Delta t(\delta/|\mathbf{a}|)(1 - \text{proj}_{\mathbf{a}}\mathbf{p}/|\mathbf{p}|). \quad (5)$$

Equation (5) simply distributes the delay reduction over all the TZs involved in the direct. Notice that for flights on a direct, the value of δ will be negative. As a result, $d_{dir}(t)$ will most often be negative indicating a delay reduction due to a direct. The projection in Eq. (5) shows that the maximum delay reduction will occur only when the flight follows the direct path \mathbf{a} between waypoints. Angular deviations between \mathbf{p} and \mathbf{a} diminish the delay reduction measured in Eq. (5).

Example Referring to Figure 4, assume that the actual distance flown $|\mathbf{a}|$ is 20 nmi and the planned distance S is 30 nmi. Then $\delta = -10$ nmi from Eq. (4). Assuming the actual flight path parallels \mathbf{a} and $\Delta t = 1$ minute, then the delay reduction during each minute of flight along the direct is computed from Eq. (5) as,

$$d_{dir}(t) = -1/2 \text{ minute.}$$

A delay reduction of half a minute is logged for each minute along the direct. So if for example, the flight takes 3.0 minutes to traverse **a**, then the net delay contribution from the direct would be -1.5 minutes. Had this flight instead followed **s** while maintaining the same groundspeed, it can be shown that the travel time would have been 4.5 minutes to cover the longer distance. Therefore, the difference between the planned and actual flight times of 4.5 and 3.0 minutes, respectively, is accounted for by the methods illustrated in this example.

Airspeed Controls

Airspeed controls occur when pilots are instructed by ATC to adjust their airspeed. This method of controlling airborne traffic may be used independently or in combination with vectoring to maintain safe separation, sequencing arrivals, or managing en route demand. Airspeed controls were detected by comparing the actual airspeed v_a to the intended airspeed v_i as expressed in the filed flight plan. Delays from airspeed controls were then defined as,

$$d_{asp}(t) = \Delta t(1 - v_a(t)/v_i). \quad (6)$$

For example, a flight intending to cruise at 450 knots that actually flew at 405 knots would experience 0.1 minutes (6 seconds) of delay per minute of flight using Eq. (6).

Airspeed is not included as a field in the ETMS TZ messages. Thus, airspeed was estimated using the reported groundspeed, and the observed winds aloft data available in the Rapid Update Cycle (RUC) weather model data. RUC data provides hourly winds aloft information for a 3D grid over the contiguous United States. Due to known issues with the ETMS altitude data from the TZ messages [9], we developed a filtering-smoothing algorithm to produce a more accurate altitude profile as demonstrated in **Figure 5**. The improved altitude profile was then used to map 4D flight positions to winds aloft at a particular time, position, and altitude. A smoothing algorithm was also applied to the TZ groundspeed data before computing v_a .

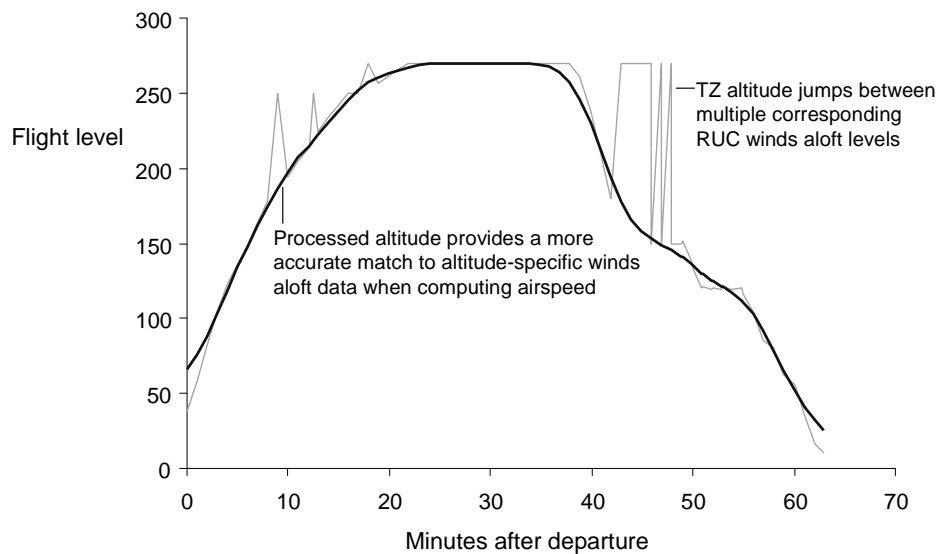


Figure 5. A filtering-smoothing algorithm was developed and implemented to produce a more realistic altitude profile for matching flight positions to winds aloft data

The filed airspeed v_i was considered to represent the desired airspeed in the absence of ATC intervention for flights at cruising altitude. Cruising altitude, according to our subject matter experts, refers roughly to flight levels 240 and above. Therefore, we contained our search for airspeed controls to flights at cruising altitude where the filed airspeed was a reasonable approximation of pilot intent. Limitations of this current approach to measuring airspeed controls include cases where pilots slow down due to turbulence or during the portion of ascent and descent profiles that occur at or above flight level 240. In these scenarios, deviations between the actual and planned airspeeds would not be a result of ATC delay, but rather the intent of the pilot.

Amendments

The final component of airborne delay included in our mathematical model comes in the form of airborne amendments. Airborne amendments occur when ATC assigns a revised route to an airborne flight. About half of all flights have their routes amended while airborne. Amendments contribute to airborne delay in that the distance and time required to reach the destination may change. During periods of heavy congestion for example, ATC may off-load demand to other regions of airspace by issuing amendments to flights bound for the congested region. The distance added or subtracted as a result of an airborne amendment affects the flight time required to reach the destination. This change in required flight time is measured here as amendment delay.

It is a relatively simple calculation to determine the change in remaining distance along the route when an airborne amendment is issued. The change in remaining flight time, however, cannot be defined at the moment the amendment is issued because this depends on the future groundspeed along the new route. Therefore, delays associated with amendments were estimated based on the change in remaining distance and an estimate of future groundspeeds. An estimated groundspeed profile was constructed for each flight based on assumed parameters such as runway groundspeed v_r as well as constant rates of acceleration a_a and deceleration a_d . Constraints from the filed flight plan, including the route length L and estimated flight time t_{ete} , were incorporated as shown in **Figure 6** where t_a is the time spent accelerating, t_c is the time in cruise, and t_d is the deceleration time.

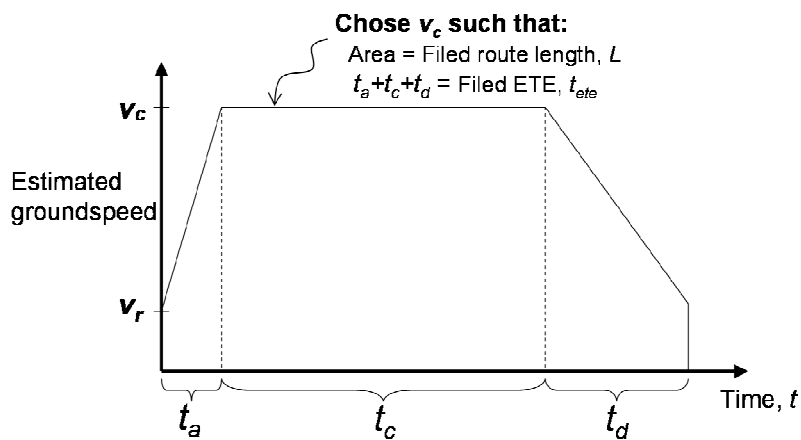


Figure 6. Estimated groundspeed profile used to estimate the impact on flight time of changes in remaining distance due to airborne amendments.

The final step in establishing an estimated groundspeed profile for each flight was to define a reasonable estimate for the groundspeed during cruise, v_c . For simplicity, winds aloft were assumed to be constant with respect to the planned route, which allowed for them to be dropped from the equations. For all of its apparent simplicity, this model appears to be relatively accurate and is documented further in [1].

The value of v_c is then identified so that the area under the estimated groundspeed profile equals L and the duration of flight equals t_{ete} , thus satisfying the constraints of the filed flight plan. This computation was completed by defining the distance flown D based on the area under the groundspeed profile as a function of one variable t_a , which can be shown to be,

$$D(t_a) = [-(a_a/2)(1 + a_a/a_d)]t_a^2 + [a_a t_{ete}]t_a + v_r t_{ete}. \quad (7)$$

The quadratic equation was then used to solve for t_a so that D , which has units of distance, equals the length of the filed route,

$$D(t_a) - L = 0. \quad (8)$$

After solving for t_a , the cruising groundspeed is defined by,

$$v_c = v_r + a_a t_a. \quad (9)$$

All remaining parameters in the estimated groundspeed profile can now be solved for in relation to the value of t_a .

These parameters were then used in combination with the one-dimensional motion equations to create a table of estimated remaining flight time t_{rem} as a function of remaining distance D_{rem} as in **Table 1**. The estimated remaining flight time was computed for each nautical mile remaining along the route.

Table 1. Example of estimated remaining flight time as a function of remaining distance used in computing delay associated with airborne amendments

Remaining Distance (nmi) D_{rem}	Est. Remaining Flight Time (min) t_{rem}
0	0
1	0.32
2	0.62
3	0.88
⋮	⋮
L-2	185.3
L-1	185.6
L	t_{ete}

The delay attributed to an airborne amendment was defined by the change in estimated remaining flight time associated with the change in remaining distance between the previous and current routes, r_{i-1} and r_i respectively,

$$d_{amd}(t) = t_{rem}(D_{rem}(r_i(t))) - t_{rem}(D_{rem}(r_{i-1}(t))). \quad (10)$$

This is to say that the remaining flight time was estimated at time t along the amended route r_i and again along the previous route r_{i-1} . Amendment delay was then defined by the change in estimated remaining flight time between these two routes.

Combining Components of Airborne Delay

This approach to measuring airborne delay detects and measures four distinct types of delay; vectoring, directs, airspeed controls, and amendments. Each of these delay components may be analyzed individually or combined to measure the net airborne delay imposed on a flight for each TZ message. Equation (11) defines the net airborne delay for a flight at time t where $d(t)$ is the amount of delay incurred since time $t-\Delta t$,

$$d(t) = d_{vect}(t) + d_{dir}(t) + d_{asp}(t) + d_{amd}(t). \quad (11)$$

Algorithm Development

An algorithm was developed to implement the methods described above for computing airborne delays. The current algorithm computes airborne delays at a rate of around 120,000 TZ messages per minute and has been applied to two year's worth of ETMS flight data, which equates to roughly 4 billion TZs to date.

III. Results

A number of methodologies for evaluating and visualizing the airborne delay data have been developed. In this section we present preliminary results of our ongoing analysis of airborne delay patterns.

Types of Airborne Delay

Table 2 shows the distribution of net airborne delay over the four types of delay being measured. These results comprise the approximately 1.8 million ETMS flights having both filed flight plans and TZ data during the month of July 2005. Airborne delay statistics were computed in two categories: 1) at all altitudes and 2) above 12,000 ft. The reason for this partitioning is based on our observation that flights often undergo substantial vectoring while inside the departure and arrival terminal areas as they are directed along established departure and arrival procedures. The details of these procedures are not included in the flight plans available through ETMS. In order to separate delays

within the terminal airspace from those en route, we apply a filter of 12,000 ft which loosely corresponds to the tops of many Terminal Radar Approach Control (TRACON) facilities.

Over all altitudes, vectoring delays averaged 5.9 minutes per flight. When looking above 12,000 ft however, the per flight average is 1.8 minutes. This is an indication that the majority of vectoring delays (4.1 out of 5.9 minutes) occur below 12,000 ft. Much of this vectoring was observed near the departure and arrival airports where the ETMS route messages do not contain the standard departure and arrival procedures as described above. Directs have less of an impact on flight progress averaging less than one minute of delay reduction per flight. Statistics for airspeed controls are consistent between both altitude categories because, as previously described, airspeed controls are only measured above FL240.

Table 2. Airborne delay by type and altitude during July 2005

Type of airborne delay	All altitudes		Above 12,000 ft ("en route")	
	Minutes per flight	Standard deviation	Minutes per flight	Standard deviation
Vectoring	5.9	10.8	1.8	7.3
Directs	-0.6	7.6	-0.3	7.4
Airspeed controls	0.2	2.1	0.2	2.1
Amendments	-0.7	60.0	-0.6	43.6
Total	4.8	61.4	1.1	44.9

The average delay from amendments is also relatively low in magnitude. However, the relatively large standard deviation (60.0 minutes at all altitudes, 43.6 minutes above 12,000 ft) indicates that amendments have a significant impact on airborne delay. Upon further analysis, we found many flights underwent large route amendments just after departure. For example, the ORD-bound flight in **Figure 7** had a filed route of length 1,013 nmi shown in black. Once airborne, an amendment was issued placing the flight on a more direct path and reducing the remaining distance to the destination by 363 nmi. Equation (10) was used to estimate a 57-minute delay reduction associated with this amendment. About half of the flights in July 2005 experienced at least one route amendment. Of those flights, 73% had a net delay reduction from amendments, while the remaining 27% had delay increases. Whereas

vectoring delays are always positive, the distribution of amendment delay between negative and positive values contributes to its relatively large standard deviation.

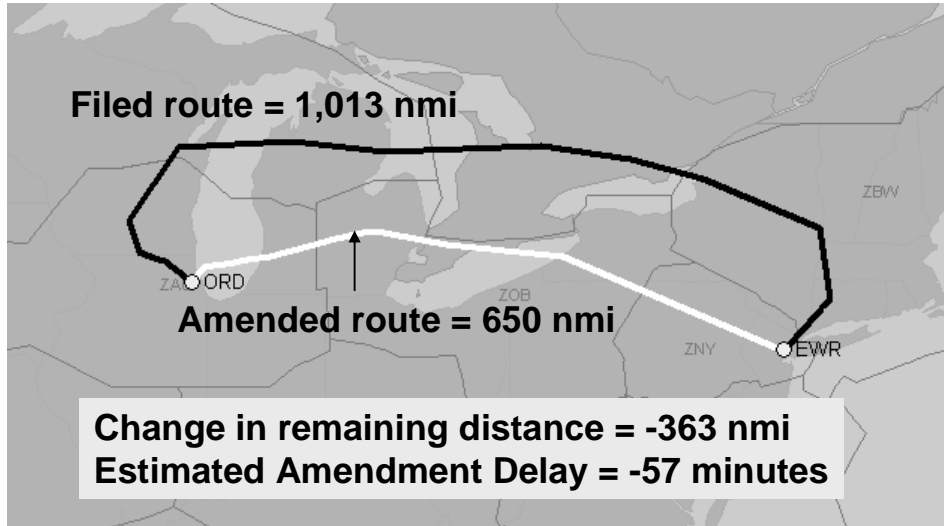


Figure 7. Route amendments can have a significant impact on airborne delay

Validating Measurement of Vectoring Delays

Figure 8 shows actual ETMS data of the flown path and active route of a flight undergoing circular holding as it approaches the destination. The entry and exit points of circular holding patterns are typically in close proximity to one another, enabling a basic validation of the approach to measuring vectoring delays.

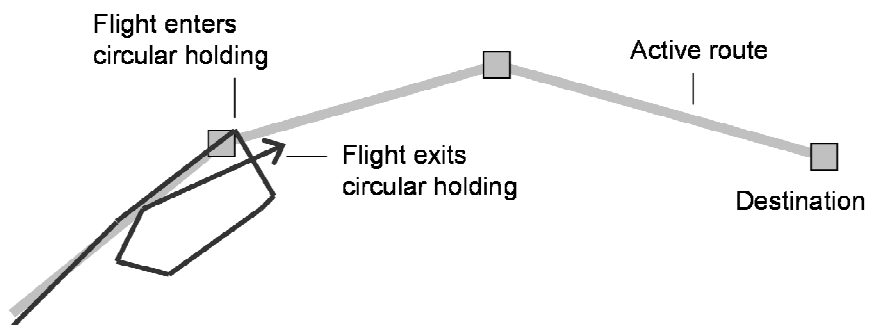


Figure 8. Flight undergoing circular holding depicted from ETMS data

As the name suggests, circular holding involves the vectoring of a flight through a complete circular race-track type motion. As a result, the flight makes no net forward progress along the route, meaning the entire time spent in

the holding pattern is incurred as vectoring delay. Vectoring delay estimates were validated by comparing the measured vectoring delay accumulation to the time spent in holding. **Figure 9** shows the cumulative vectoring delay for the flight mentioned in **Figure 8**. This flight spent approximately 8.5 minutes in the circular holding pattern, during which time our algorithm detected 8.5 minutes of vectoring delay.

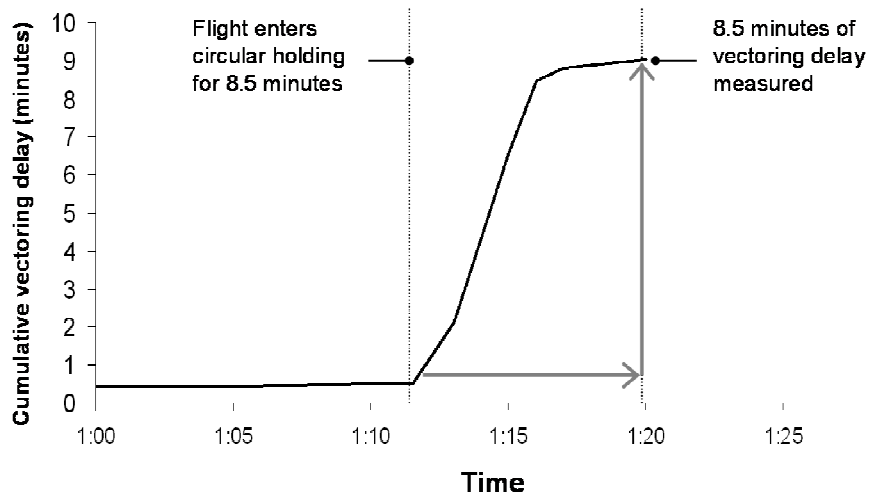


Figure 9. Vectoring delay accumulation during circular holding should equal the time spent in holding since no net forward progress is made along the active route. Algorithm results for the flight track shown in Figure 8 were validated by a match between vectoring delay and time in holding for this flight.

Analyzing Multiple Components of Airborne Delay

This new approach to measuring airborne delay enables a unique look into delay causality in terms of ATC vectoring, airspeed controls, directs and amendments. For example, the ORD-bound flight in **Figure 10** experienced 21 minutes of airborne delay. How much of this delay can be attributed to vectoring as opposed to amendments, directs versus speed controls? To answer these types of questions, we explored the four components of airborne delay through the history of this flight.

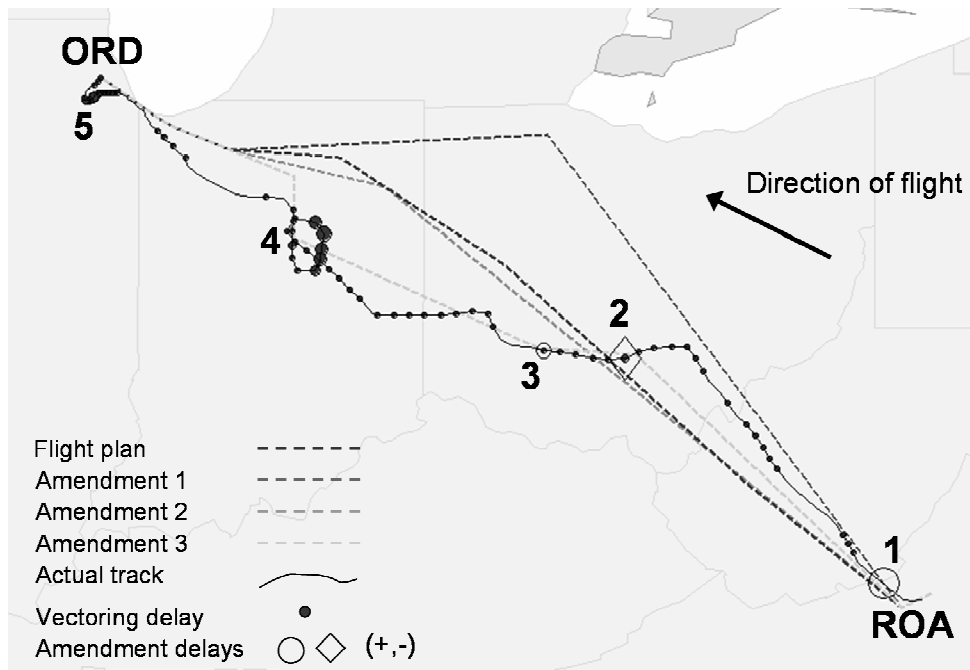


Figure 10. Airborne delay for an ORD-bound flight

Label 1: 1825Z. Shortly after departing out of ROA, the open circle marks where the active route was changed from the filed flight plan to Amendment 1. The area of the open circle represents the additional delay incurred from this amendment. The increase in remaining distance associated with this amendment was detected and measured as 6 minutes of airborne delay based on Eq. (10).

Label 2: 1853Z. After flying parallel Amendment 1, which equates to no vectoring delay, the flight was vectored west and assigned to Amendment 2. The diamond at label 2 indicates a delay reduction of 7 minutes based on Eq. (10), which follows from the observed reduction in remaining distance to the destination. Vectoring in proximity to label 2 is indicated by closed dots with the area of each dot representing the amount of vectoring delay measured between consecutive TZ messages using Eq. (2).

Label 3: 1858Z. The final amendment added about 1 minute of delay to the flight, reflected in the relatively small open circle. Between 1900Z and 1930Z, the airspeed was reduced from the filed airspeed of 439 knots to an average of 420 knots. This speed control contributed just over one minute of delay based on Eq. (6).

Label 4: 1921Z. While on Amendment 3, the flight was vectored through a circular hold. As in the previous section, vectoring delay measurements were validated by comparing the measured delay to the time spent in circular holding. The flight spent 8 minutes in circular holding at label 4 during which time 8 minutes of vectoring delay were measured using Eq. (2). Immediately after exiting the holding pattern, the flight takes a relatively direct path towards ORD, resulting in a 2-minute delay reduction.

Label 5: 1954Z. The flight is vectored to line up for final approach into ORD. This vectoring delay is shown again using the closed dots.

Figure 11 shows the cumulative airborne delay for the flight analyzed in **Figure 10** where airborne delay includes the combined effect from vectoring, directs, airspeed controls, and amendments.

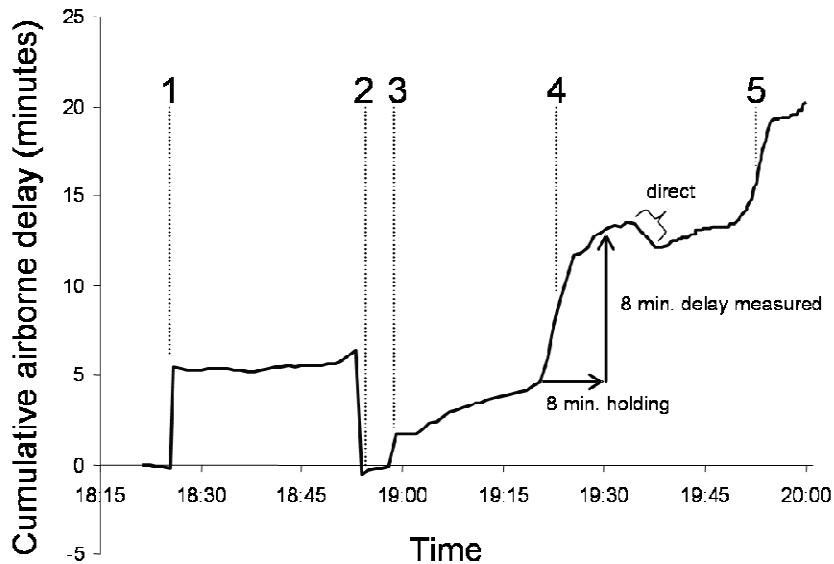


Figure 11. Cumulative airborne delay for the flight shown in Figure 10

Time labels 1 through 5 in **Figure 11** correspond to the position labels in **Figure 10**. For example, Label 1 indicates the place and time of the first airborne amendment, adding 6 minutes of airborne delay. The relatively flat slope between Labels 1 and 2 in **Figure 11** indicates the absence of airborne delay as the flight travels parallel Amendment 1 in **Figure 10**. The circular holding at Label 4 is followed by a small direct towards Label 5. The 21 minutes of airborne delay incurred by this flight were attributed to:

- Vectoring: 22 min

- Direct: -2 min
- Airspeed Controls: 1 min
- Amendments: no net delay from the 3 amendments

Patterns of Airborne Delay

The previous section examined the composition of airborne delay for a single flight. In this section however, delays from many flights are analyzed to help identify spatial patterns of airborne delay. Two scenarios are presented in this section: 1) a day having nominal airborne delay and 2) a day when significant airborne delays occurred. The dates and time ranges for the two scenarios are as follows:

Scenario 1: ORD arrivals on Tuesday August 16, 2005 from 12:00 Z-15:59Z

Scenario 2: ORD arrivals on Thursday August 4, 2005 from 12:00 Z-15:59Z

Note that both scenarios cover the same time of day. **Figure 12** shows the actual paths flown for the 194 ORD arrivals in Scenario 1 during which time airborne delays were relatively minimal. The majority of traffic is seen funneling inbound along nearly-radial paths stretching out from the four arrival fixes.

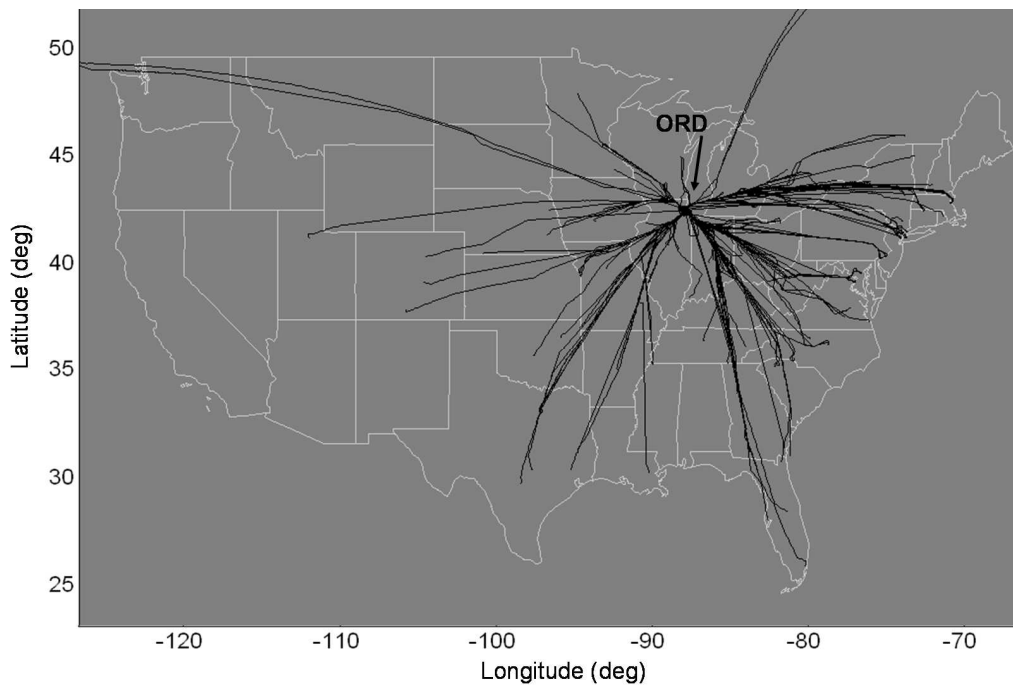


Figure 12. Flown paths for ORD arrivals in Scenario 1: August 16, 2005 1200Z-15:59Z.

The dot technique of representing airborne delay on a map, introduced in **Figure 10**, is limited when it comes to displaying delays from large numbers of flights as the dots tended to overlap on top of one another. A preferable technique in such cases is to aggregate airborne delays over a NAS-wide grid and then shade the grid cells based on the amount of delay they contained. **Figure 13** applies this technique in showing airborne delays from vectoring, directs, and airspeed controls for the Scenario 1 flights.

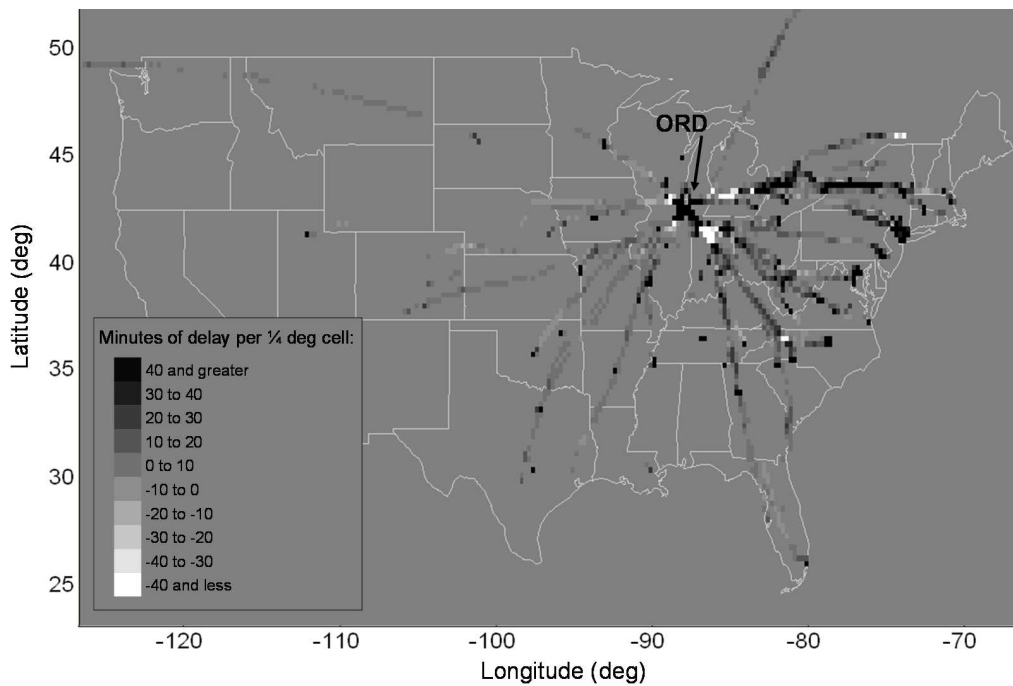


Figure 13. Airborne delay in ¼ deg grid cells for Scenario 1 flights. Shades darker than the background indicate a positive net delay. Lighter shades show delay reduction, mainly due to directs.

The darkest cells in **Figure 13** indicate locations where the total airborne delay exceeded 40 minutes during the four-hour period starting at 12:00Z on August 16, 2005. A region of significant airborne delay is visible around ORD, which was found to typically correspond with vectoring applied while lining up flights for final approach. Delays are also common near the departure end of each flight track where flights are vectored relative to their active route. As previously discussed, ETMS route messages does not contain information on the specific departure procedure a flight intends to use; only a string of waypoints is provided. This means that the actual pilot intent, which could include a standard departure procedure specific to the departure airport runway configuration, is not always represented completely in the ETMS waypoint string. Care must be taken in interpreting airborne delays within close proximity to the origin and destination. Airborne delays are also detected just east of Michigan, propagating east towards Boston. Referring back to **Figure 12**, this area of airborne delay corresponds to a number of flights experiencing significant path-stretching vectoring delay as flows from Canada, Boston, and New York are merged together.

Delay reductions appear in lighter shades. One such area appears just southeast of ORD. This region, in which the total airborne delay was measured to be less than zero, corresponds with a commonly-occurring observation of flights arriving over BEARZ. As flights approach BEARZ from the south and southeast, the active route typically takes a slight left hand turn to the northwest for approach into ORD. Flights are often observed taking a shortcut across this bend in the route. These shortcuts result in a reduction of distance flown, which is equated to a time savings based on Eq. (5).

Scenario 2 was selected to highlight the drastic contrast in flight paths and airborne delays that can occur on different dates. **Figure 14** shows actual flight paths for ORD arrivals on Thursday August 4, 2005 during the same time of day as in the previous scenario; 12:00Z-15:59Z. The flow of traffic differs significantly from the “baseline” scenario. Notice the large number of east coast departures, from Maryland to Georgia, that are being moved from the southeast arrival corridor to the southwest ORD arrival fix, PLANO. This movement of flights results in large amounts of airborne delay, which are detected and displayed in **Figure 15**.

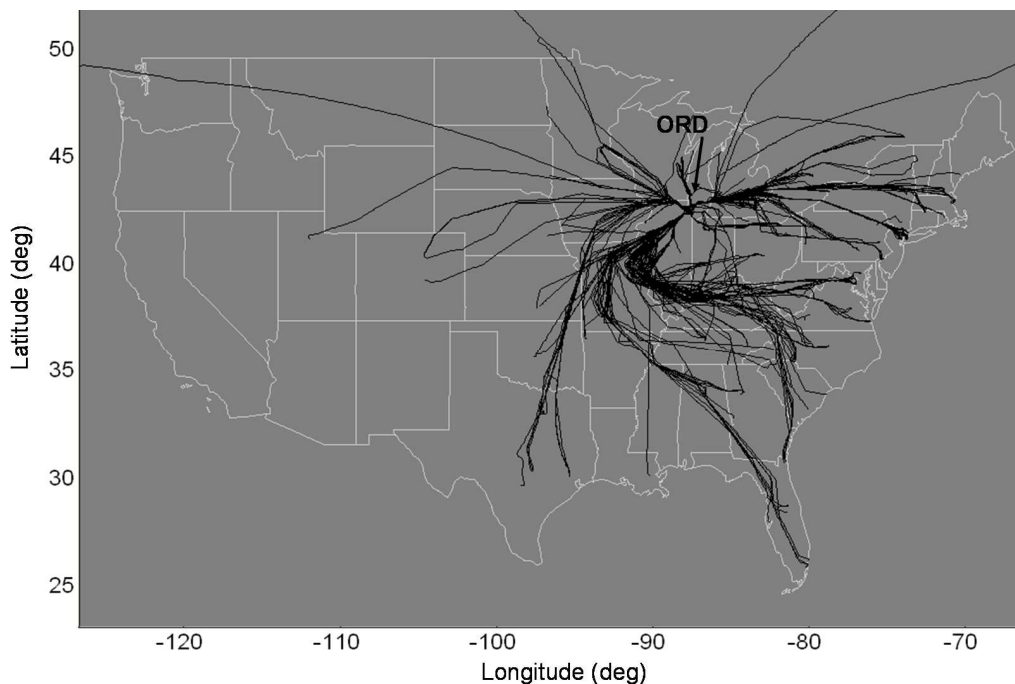


Figure 14 Flown paths for ORD arrivals in Scenario 2: August 4, 2005 1200Z-15:59Z.

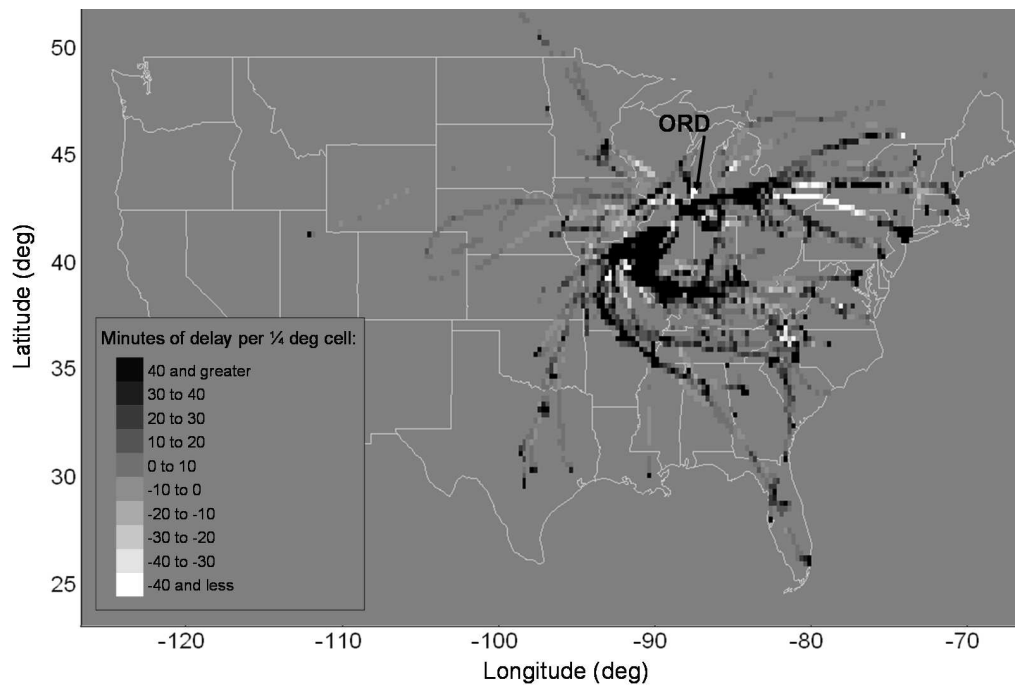


Figure 15 Airborne delay in ¼ deg grid cells for Scenario 2 flights. Large regions of airborne delay are measured as flights are off loaded from the southeast to the southwest of ORD.

Analyzing airborne delays in this way allows for the study of where and when these delays are occurring. It is also possible to compare the composition of these delays for scenarios 1 and 2 as shown in **Table 3**. The number of ORD arrivals increased 48% from 194 to 287 flights. Airborne delay per flight increased from 4.1 to 21.1 minutes and the number of amendments rose from an average of 0.9 to 2.4 per flight. Airborne delays were further dissected into their four types. Minimal change was detected in the airspeed controls. The other three types of delay each showed an increase in magnitude. For example, vectoring delays increased from about 4.9 to 8.0 minutes per flight. In Scenario 1 there were only 176 airborne amendments having a net delay reduction of 110 minutes. The number of amendments in Scenario 2 rose to 692 adding nearly 4,000 minutes of airborne delay for the 287 ORD arrivals; nearly 14 minutes per flight. Many of these additional amendments were issued for what appears to be the fix-balancing of flights from ORD's southeast arrival fix, BEARZ, to the southwest fix, PLANO, evident in the flight tracks shown in **Figure 14**.

Table 3 Comparison of airborne delay summary for scenarios 1 and 2 – ORD arrivals 12:00Z-15:59Z on August 16, 2005 and August 4, 2005, respectively.

	Scenario 1		Scenario 2		
	Total	Per flight	Total	Per flight	
Arrivals	194		287		flights
Airborne Delay	802	4.1	6,059	21.1	min
Vectoring	954	4.9	2,310	8.0	min
Directs	-101	-0.5	-307	-1.1	min
Airspeed Controls	60	0.3	65	0.2	min
Amendments	-110	-0.6	3,992	13.9	min
Amendment Count	176	0.9	692	2.4	

Airborne Delay Propagation and Weather

Under normal operating conditions, ATC is effective at maintaining throughput to the airport terminal areas [7]. Factors such as weather, however, can increase the complexity of the controlled airspace, resulting in increased controller workload, which may lead to further delays upstream to manage incoming traffic. According to the Aviation Capacity Enhancement Plan [8], weather is a leading cause of airborne delays greater than 15 minutes [3]. Previous research [2] has established the importance of studying patterns and causes of airborne delay propagation as a key component in the improvement of TFM procedures.

Airborne delay propagation was investigated using displays of delay as a function of distance and time as in **Figure 16**. The figure shows ORD-bound flights within 500 miles of the airport approaching over BEARZ during a 14-hour period. The figure is divided into grid cells, each 5 nautical miles in height and 2 minutes in width. These cells are shaded to reflect the amount of airborne delay incurred in each cell.

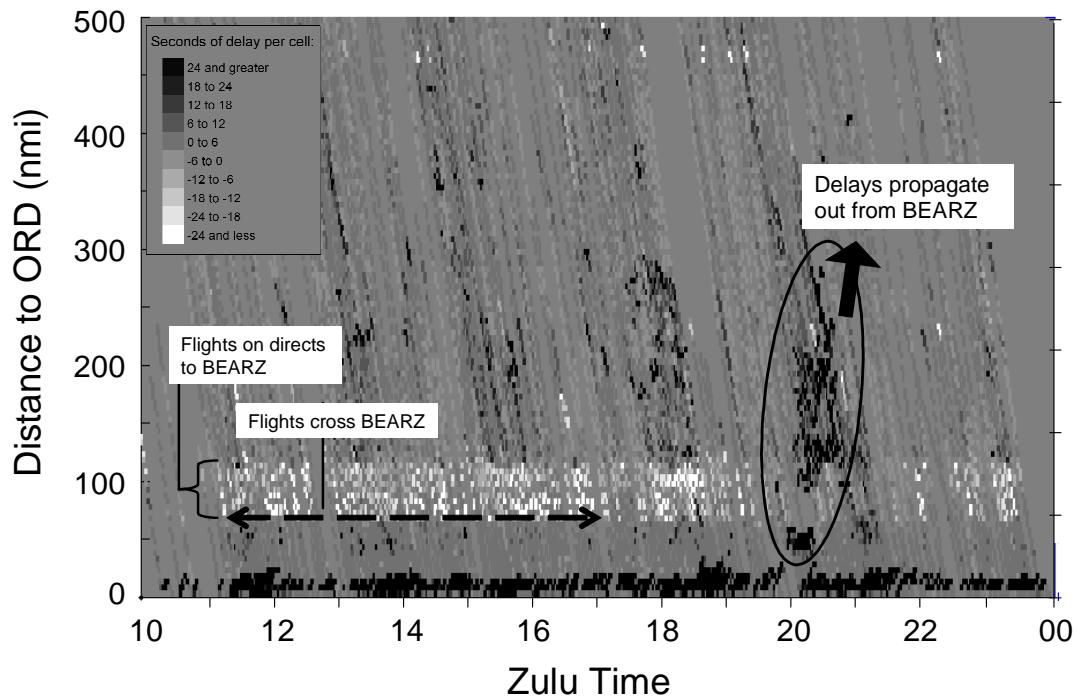


Figure 16. Airborne delay propagation for ORD BEARZ arrivals.

A prominent white band is visible at a distance of approximately 75 to 125 nautical miles from ORD. The white band, which persists for almost the entire time domain, indicates flights experiencing a delay reduction. Upon further investigation, it was discovered that this white band was caused by flights taking directs past BEARZ as in the discussion of **Figure 13**. Terminal area vectoring contributes to the pattern of darker cells along the horizontal axis. At 20Z, delays begin to appear where flights cross BEARZ, indicated by the small patch of dark cells 50 nautical miles out from ORD at the lower edge of the ellipse in **Figure 16**. These delays quickly propagate to a distance of about 300 nautical miles in a span of only 20 minutes – an implied propagation speed of 750 knots.

The impact of weather on the propagation of airborne delay was analyzed in **Figure 17**. The figure includes a simple weather index (WX index) which corresponds to the amount of National Convective Weather Detection (NCWD) weather within 50 nautical miles of the destination airport; in this case ORD.

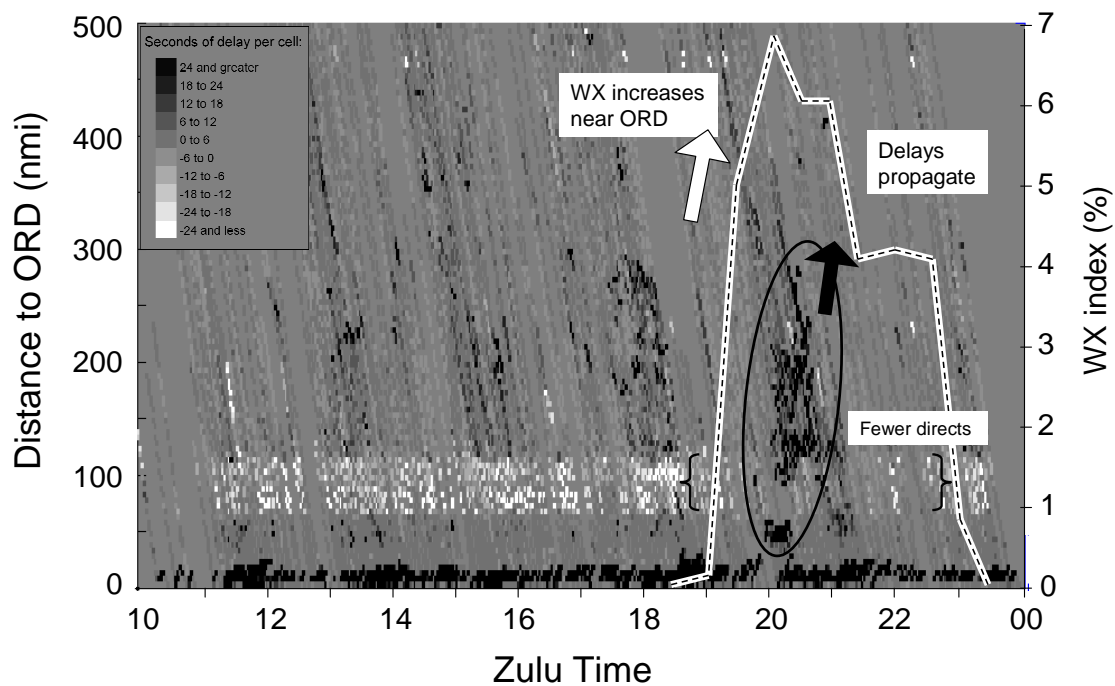


Figure 17. Airborne delay propagation for ORD BEARZ arrivals including a weather index. WX index represents the amount of NCWD weather within 50 nautical miles of ORD.

The presence of weather increases the complexity of the airspace. Airborne delays appear near BEARZ shortly after the weather comes within 50 nautical miles of ORD. **Figure 17** shows that the application of these airborne delay measurement techniques provides new insights into a range of important analyses including the role of weather on airborne delay propagation.

IV. Sources of Error and Special Cases

In developing algorithms for implementing this new approach to measuring airborne delays, we encountered various sources of error and special cases. For example, in Section II we described the use of an altitude filter-smoothing algorithm for improving the quality of TZ altitude data. In this section we describe the handling of additional errors and special cases.

Backtracking Routes

Our algorithm makes use of the ETMS WAYPOINTS field for defining the intended path of flight. This field provides latitude/longitude values associated with each waypoint in a particular route message. In some cases, the chain of waypoints defined in this field repeats or backtracks. For example, a sequence such as ABCBCD may occur (i.e. segment BC is repeated). In other cases, such as in **Figure 18**, the route may backtrack on itself with a relatively

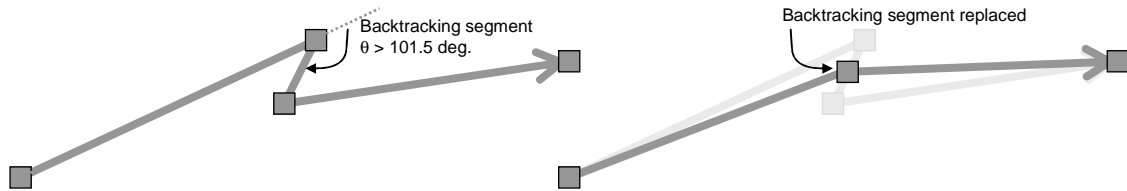


Figure 18. Repeating and backtracking waypoints are filtered out to improve the quality of vectoring delay estimates

large change in heading. Repeating or backtracking waypoint segments, which can have a negative impact on the accuracy of vectoring delay estimates, occurred in about 20% of the routes we investigated. As a result, we developed a preprocessing algorithm for filtering the waypoints prior to identifying the current waypoint segment and computing airborne delays. The filtering process is as follows:

1. Compute the absolute change in heading between consecutive waypoint segments, θ
2. If $\theta > 101.5$ degrees or $\text{acos}(-0.2)$, then the next segment is backtracking
3. Replace the endpoints of the backtracking segment with their average (see Figure 18)
4. Process the next waypoint

ETMS TZ Positions

As airborne flights cross from one facility into another, there are often periods where a flight's position is reported by two or more facilities simultaneously. TZ positions reported from multiple facilities sometimes disagree, resulting in inaccurate representations of flight trajectories as in the notional example shown in **Figure 19**. These inconsistencies in position reports could negatively impact vectoring delay estimates. In an attempt to mitigate the effects of inaccurate position data, we recently developed a TZ position filter with the following attributes:

- Periods where flight position is being reported by more than one facility are identified as “overlaps”
- These overlaps are processed to systematically interpolate and then weight reports from multiple facilities to define a more realistic trajectory
- The original number of TZ messages and message times are preserved
- A filtered 2D trajectory is computed

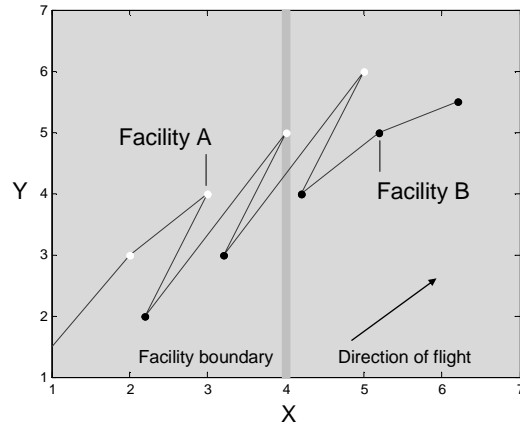


Figure 19. TZ messages originating from different facilities may produce erroneous tracks

Figure 20 shows results from applying the position filter to a LAX-bound flight in which position reports originating from different facilities appear as black or white circles. Clearly visible are the inconsistencies between reports from the two facilities. After applying the position filter, the filtered track appears to represent a more realistic trajectory through the airspace. Next steps for this research include further validation as well as utilizing the

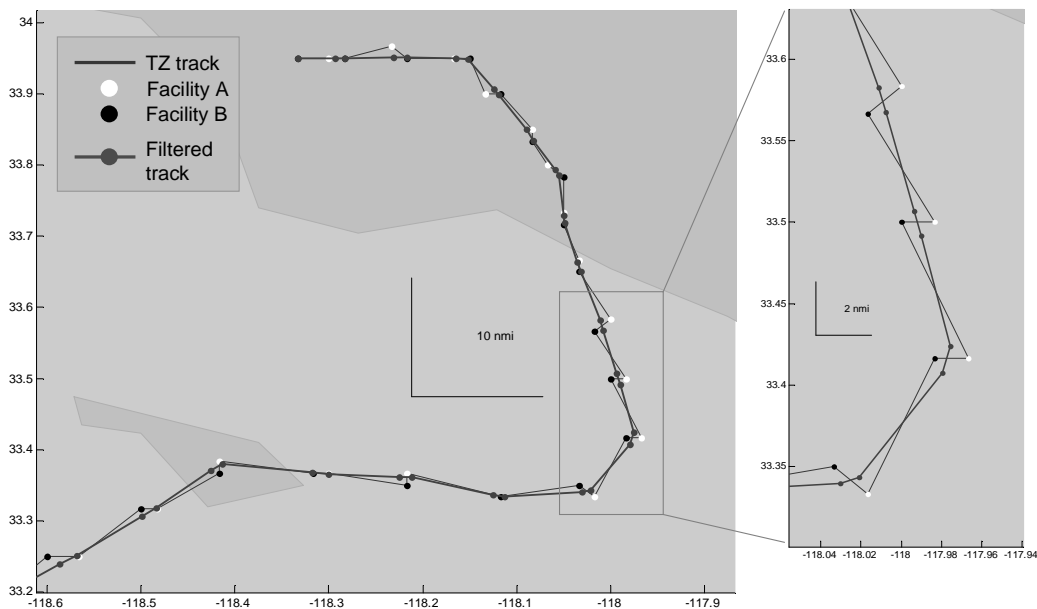


Figure 20. TZ position filter results for a LAX-bound flight on arrival

filtered track data when computing vectoring delays.

Vectoring Delays along the Final Waypoint Segment

One of the special cases handled by the airborne delay algorithm deals with vectoring near the destination. After passing the second-to-last waypoint in its route, a flight is then on the final waypoint segment as depicted in **Figure 21**. In this special case, flying parallel to the waypoint segment is no longer indicative of zero delay. Rather a direct path to the destination is optimal. We therefore reassign \mathbf{s} to be the displacement vector between the previous flight position and the destination when using Eq. (2) to estimate vectoring delays along the final waypoint segment. Based on this approach, any displacement not directed towards the destination while on the final waypoint segment will result in vectoring delay being recorded.

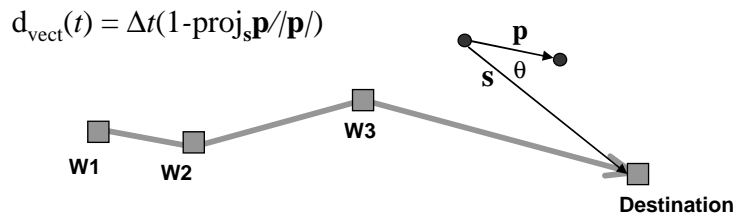


Figure 21. Vectoring delays along the final waypoint segment are measured relative to a direct path to the destination.

V. Conclusion and Future Research

We presented a methodology for measuring airborne delay in which delays are decomposed into those due to vectoring, directs, airspeed controls, and amendments. When considering all four components, airborne delays averaged 4.8 minutes per flight during July 2005. Average delays as high as 21 minutes per flight we measured during a case study of Chicago O’Hare arrivals during inclement weather. Preliminary results also indicate that vectoring is the most significant contributor to airborne delays; averaging 5.9 minutes per flight. The altitude processing algorithm presented in this paper was applied to study airborne delays by stratum. It was found that 69% (4.1 out of 5.9 minutes) of vectoring delays occur at or below 12,000 feet. Analysis of airborne delay propagation yielded initial results suggesting delays propagating upstream at 750 knots.

Additional validation of the airborne delay methodology is required. In particular, it would be valuable to compare airspeed estimates inferred using winds aloft data against those that might be obtained directly from the airlines. The position filtering algorithm we developed should be incorporated into the airborne delay processing to reduce potential errors in vectoring delay estimates stemming from inconsistent position reports. We will extend this methodology to analyze the impact of airborne delays on arrival rates during Ground Delay Programs and Airspace Flow Programs, for defining new performance metrics, and for improving flight time predictability.

Acknowledgement

This work was supported in part by CDM CE funding led by Ved Sud of the FAA.

References

- [1] Myers, T., Khorrami, B., Cross, C., Kierstead, D., "Airspace Congestion Management Research", Metron Aviation, Inc., Technical Report for FAA 32F0907-014-R0, Herndon, VA, September, 2007.
- [2] Brennan, M., and Thompson, T., "Using Historical Flight Data to Evaluate Airborne Demand, Delay and Traffic Flow Control", *Proceedings of the Fifth USA / Europe Air Traffic Management R&D Seminar*, Budapest, Hungary, 2003.
- [3] Voss, W., and Hoffman, J., "Analytical Identification of Airport and Airspace Capacity Constraints", *Proceedings of the Third USA / Europe Air Traffic Management R&D Seminar*, Napoli, Italy, 2000.
- [4] Hoffman, J., "An Examination of Excess Distances Flown in the Contiguous United States", MITRE Corporation, MITRE Product MP99W0000103, McLean, VA, 2000.
- [5] Howell, D., Bennett, M., Bonn, J., and Knorr, D., "Estimating the En Route Efficiency Benefits Pool", *Proceedings of the Fifth USA / Europe Air Traffic Management R&D Seminar*, Budapest, Hungary, 2003.
- [6] Kell, S., and Chen, Y., "Initial Design and Description for Airborne Delay Monitoring Capabilities of CAPER", MITRE Corporation, MITRE Product MP03W0000056, McLean, VA, 2003.
- [7] Krozel, J., Lee, C., and Mitchell, J.S.B. "Estimating Time of Arrival in Heavy Weather Conditions," *AIAA Guidance, Navigation, and Control Conf.*, Portland, OR, 1999, pp. 1481-1495.
- [8] Federal Aviation Administration, "1997 Aviation Capacity Enhancement Plan", Federal Aviation Administration Office of System Capacity, Washington, D.C., 1997.
- [9] Chatterji, G., Sridhar, B., Kim, D., "Analysis of ETMS Data Quality for Traffic Flow Management Decisions", *AIAA Guidance, Navigation, and Control Conf.*, Austin, TX, 2003.